



HAL
open science

Disentangling elastic relaxation and ferroelectric domain contributions to in plane X-ray scattering profile: A necessity in strained ferroelectric superlattices

M. Gharbi, C. Davoisne, F. Le Marrec, L. Dupont, N. Lemée

► To cite this version:

M. Gharbi, C. Davoisne, F. Le Marrec, L. Dupont, N. Lemée. Disentangling elastic relaxation and ferroelectric domain contributions to in plane X-ray scattering profile: A necessity in strained ferroelectric superlattices. *Materials Letters*, 2020, 275, pp.128138 -. 10.1016/j.matlet.2020.128138 . hal-03490854

HAL Id: hal-03490854

<https://hal.science/hal-03490854>

Submitted on 21 Jun 2022

HAL is a multi-disciplinary open access archive for the deposit and dissemination of scientific research documents, whether they are published or not. The documents may come from teaching and research institutions in France or abroad, or from public or private research centers.

L'archive ouverte pluridisciplinaire **HAL**, est destinée au dépôt et à la diffusion de documents scientifiques de niveau recherche, publiés ou non, émanant des établissements d'enseignement et de recherche français ou étrangers, des laboratoires publics ou privés.



Distributed under a Creative Commons Attribution - NonCommercial 4.0 International License

1 **Disentangling elastic relaxation and ferroelectric domain contributions to in plane**
2 **X-ray scattering profile: a necessity in strained ferroelectric superlattices**

3 M. Gharbi¹, C. Davoisne², F. Le Marrec¹, L. Dupont^{2,3} and N. Lemée^{1*}

4 ¹Laboratoire de Physique de la Matière Condensée, UR 2081, University of Picardie
5 Jules Verne, 80039 Amiens, France

6 ²Laboratoire de Réactivité et de Chimie des Solides, UMR CNRS 7314, University of
7 Picardie Jules Verne, 80000, Amiens, France

8 ³Plateforme de Microscopie Électronique, University of Picardie Jules Verne, 80000,
9 Amiens, France.

10 *Corresponding author: nathalie.lemee@u-picardie.fr

11

12 **Abstract**

13

14 Ferroelectric nanodomains give rise to diffuse X-ray scattering peaks in ultrathin films.
15 Here we study a $\text{Pb}(\text{Zr}_{0.2}\text{Ti}_{0.8})\text{O}_3/\text{SrTiO}_3$ superlattice, using X-ray diffraction and
16 transmission electron microscopy, We show that both elastic relaxation and ferroelectric
17 nanodomain structuration can contribute to distinct satellite peaks in the X-ray scattering
18 pattern. We show that transmission electron microscopy is required to disentangle elastic
19 relaxation and ferroelectric domain contributions to the in plane X-ray scattering profile.

20

21 **Keywords:** Ferroelectrics, superlattice, thin films, domain structure, X-ray scattering

22

23 **1. Introduction**

24

25 Ferroelectric nanostructures are expected to contribute to increase storage densities for
26 ferroelectric memories, and to device miniaturization. For fundamental physics, they
27 constitute fascinating objects to understand ferroelectricity at the nanoscale, since low
28 dimensionality gives rise to new phenomena. In particular as a ferroelectric film becomes
29 thinner, the density of the domains and the domain walls increases and this can play a
30 key role in the functional properties as, for example, in the negative capacitance effect
31 which has recently attracted much attention [1]. Considering a uniformly out of plane
32 polarized material, the polarization discontinuity at the film boundaries creates a
33 depolarizing field that counteracts the polarization. When the screening by free charges
34 is not effective, the stability of the polar phase is preserved by forming a 180° stripe
35 domain of alternate up and down polarization that produces characteristic features in the
36 x-ray scattering pattern [2]. Indeed, the phase contrast between the areas of up and
37 down polarization produces a modulation of the structure factor perpendicular to the
38 domain walls, and is at the origin of satellite peaks. This 180° domain structure has thus
39 been evidenced in ferroelectric thin films [2,3] as well as in ferroelectric/paraelectric
40 superlattices (SLs) [4 – 5]. However, such in-plane modulation can also result from
41 periodic structural defects [6 - 7] or ferroelastic domains [8 - 9] created to minimize the
42 elastic energy. Here we illustrate this point through the study of a $\text{Pb}(\text{Zr}_{0.2}\text{Ti}_{0.8})\text{O}_3 / \text{SrTiO}_3$
43 SL. Transmission electron microscopy (TEM) and x-ray diffraction (XRD) investigations
44 are combined to disentangle the contributions of the elastic relaxation from the
45 ferroelectric domains structure.

46

47 **2. Experimental details**

48

49 The $\text{Pb}(\text{Zr}_{0.2}\text{Ti}_{0.8})\text{O}_3 / \text{SrTiO}_3$ SL was grown starting with a PZT layer, on a single
50 crystal TiO_2 terminated (001) SrTiO_3 (STO) substrate, by pulsed laser deposition using
51 a KrF excimer laser ($\lambda = 248$ nm) and ceramic targets of SrTiO_3 (STO) and
52 $\text{Pb}_{1.1}(\text{Zr}_{0.2}\text{Ti}_{0.8})\text{O}_3$ (PZT 20/80). This SL, with wavelength 4.5 nm, is composed of 10
53 bilayers, each consisting of 5 unit cells of PZT and 6 of STO, which we designate as
54 $[\text{PZT}_5/\text{STO}_6]_{10}$. The PZT 20/80 and STO layers were deposited at 690 °C in 0.1 mbar of
55 O_2 , with a laser fluence of 2 $\text{J}\cdot\text{cm}^{-2}$ and a pulse rate of 2 Hz. Structural analysis was
56 performed on a high resolution D8 Discover Bruker diffractometer (Cu $K\alpha_1$ radiation,
57 1.5406 Å). Temperature measurements were carried out in air from room temperature
58 up to 600°C, using a high temperature XRD-chamber. All measurements were
59 reproducible after thermal cycling. The lattice parameter was determined by tracking
60 satellites peaks around the (002) reflection. Microstructural characterization was
61 performed using a TECNAI F20-S-Twin operating at 200kV equipped with a Scanning
62 Transmission Electron Microscope (STEM) function, and a High Angle Annular Dark
63 Field (HAADF) camera giving an image contrast based on atomic number. The cross
64 section samples were prepared by a focused ion beam (FIB) technique after depositing
65 a carbon/platinum bilayer to protect the surface from sputtering.

66

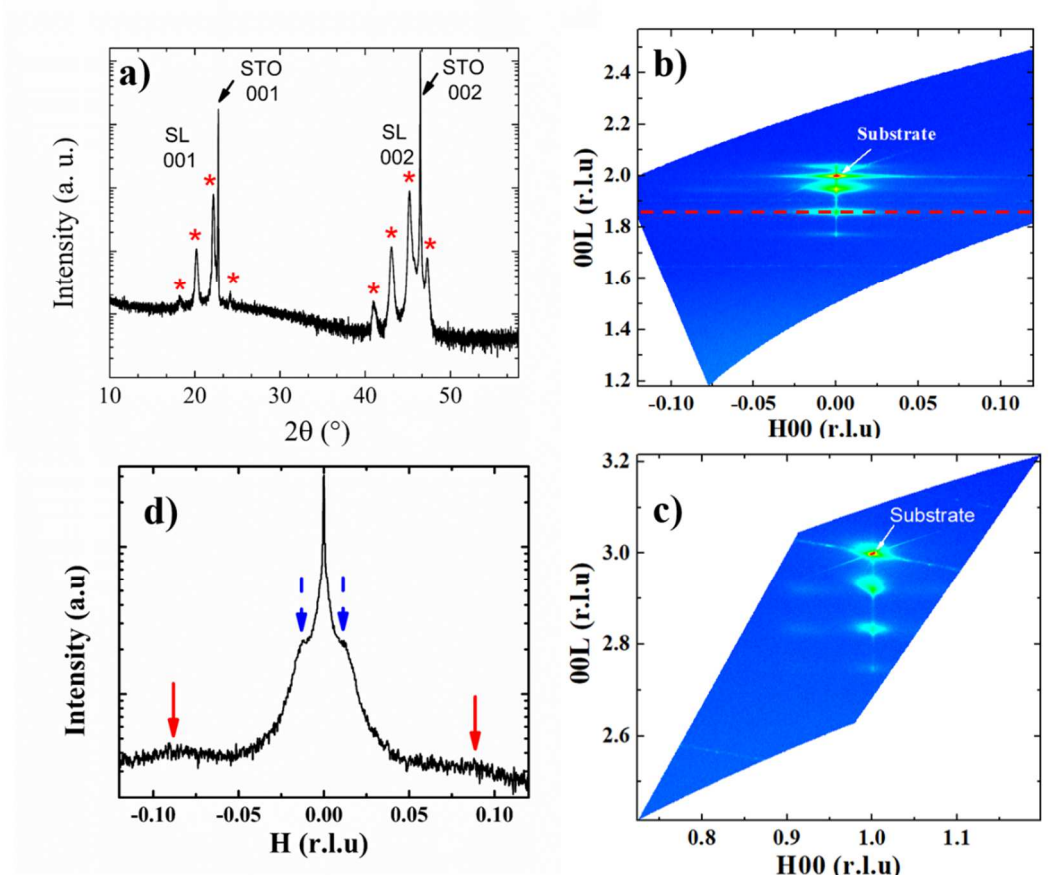
67 **3. Results and discussion**

68

69 Figure 1 displays the XRD characterizations of a $[\text{PZT}_5/\text{STO}_6]_{10}$ SL. The satellite
70 peaks detected in the θ - 2θ scan (Fig. 1a) and in the reciprocal space map (RSM) along
71 the [00L] direction (Fig. 1b), are indicative of chemical modulation along the growth
72 direction. Due to the in-plane lattice mismatch (-1.2%) between the PZT layers and STO
73 substrate, elastic relaxation by surface roughening, plastic relaxation by dislocations or
74 by the formation of ferroelastic domains can occur. Indeed when both elastic and

75 depolarization effects compete with each other, it can lead to a polydomain structure
76 consisting of polarized out of plane c- domains and in plane a- domains [9]. Here,
77 however, the reflections are related only to ferroelectric c- domains. In-plane RSM (Fig.
78 1c) shows almost coherent growth of the SL to the substrate.

79 Due to the ferroelectric/paraelectric nature of the $[\text{PZT}_5/\text{STO}_6]_{10}$ SL, a 180° stripe
80 ferroelectric domain structure is expected to minimize the depolarizing field. These
81 nanodomains can give rise to an in-plane satellite peaks detectable in x-ray scattering
82 perpendicular to the domain walls [10]. The diffraction profile along the $[\text{H}00]$ direction
83 (Fig.1d) indicates a complex profile including two types of in-plane modulation. At first
84 sight, the two peaks close to the main Bragg peak could be interpreted as the signal of
85 an in-plane modulation due to the 180° stripe nanodomain structure, corresponding to
86 an average period of 34 nm. Nanodomains are expected to originate from the
87 ferroelectric layers which consist of 5 unit cells. A domain period of 5 nm and 9 nm was
88 respectively reported in a $\text{PTO}_5/\text{STO}_5$ SL [11] and in a tricolor SL $[\text{PT}_9/\text{STO}_2/\text{PZT}_{10}]_{20}$ [5],
89 showing the dependence of the domain period on the thickness of the ferroelectric layer.
90 The value of 34 nm is therefore well above what could be expected in a 5 unit cell thick
91 PZT layer: the origin of this 34 nm period must arise from another source. In Fig. 3d (also
92 visible in fig. 3c) a second modulation of very low intensity, around $h = \pm 0.09$,
93 characterizes a period of around 4.5 nm, coherent with a modulation due to the polar
94 stripe nanodomain structure. The peaks are weak but the domain randomness
95 contributes to their smearing out. [10].



96

97

98

99 **Fig. 1.** XRD investigations of a $[PZT_5/STO_6]_{10}$ SL : (a) $\theta - 2\theta$ XRD : the asterisks indicate
 100 the satellite peaks, RSM around the (002) (b) and (103) reflection (c), (d) the diffraction
 101 profile along the [00H] direction corresponding to the dotted line on the RSM. The plain
 102 and dotted arrows indicate, respectively, ferroelectric domains and elastic relaxation.
 103 The RSM is plotted in reciprocal-lattice units with respect to the substrate lattice
 104 parameter (3.905 Å).

105

106 To further explore the 34 nm periodicity, TEM investigations have been carried
 107 out on this SL to determine if it could be produced by an ordered arrangement of
 108 structural defects. The images displayed in Fig. 2 confirm the absence of a- domains, as
 109 no characteristic domain walls between a- and c- phases are evidenced [9]. In Fig. 2b,

110 the arrangement of alternating white (higher atomic number Z, PZT layers) and grey

111 layers (lower Z, STO layers), confirms the SL periodicity along the growth direction. An

112 almost periodic wave-like modulation with an average period of around 34 nm (+/- 8 nm)

113 is also observed and is coherent with the value estimated from the XRD investigation.

114 This modulation is undoubtedly at the origin of the two satellite peaks close to the Bragg

115 peak in Fig. 1d. Such wave-like modulations have already been reported in SLs

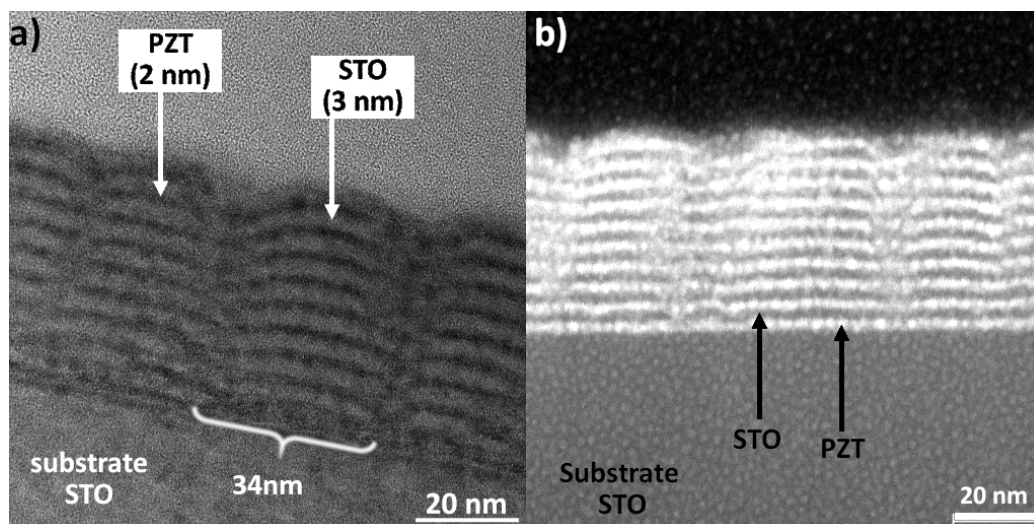
116 characterized by a significant mismatch between the materials involved in the

117 heterostructure [12,13]. Indeed, in these structures, strain is relieved through elastic

118 relaxation by surface roughening. All buried layers grown under stress contribute to the

119 surface roughness.

120



121

122 **Fig. 2.** (a) TEM micrograph of the PZT/STO SL in which the darker (greyer) layers

123 correspond to PZT (STO) and b) associated STEM-HAADF image which is of opposite

124 contrast to the TEM image.

125

126 Indirect additional evidence for the existence of a polar nanodomain structure in the

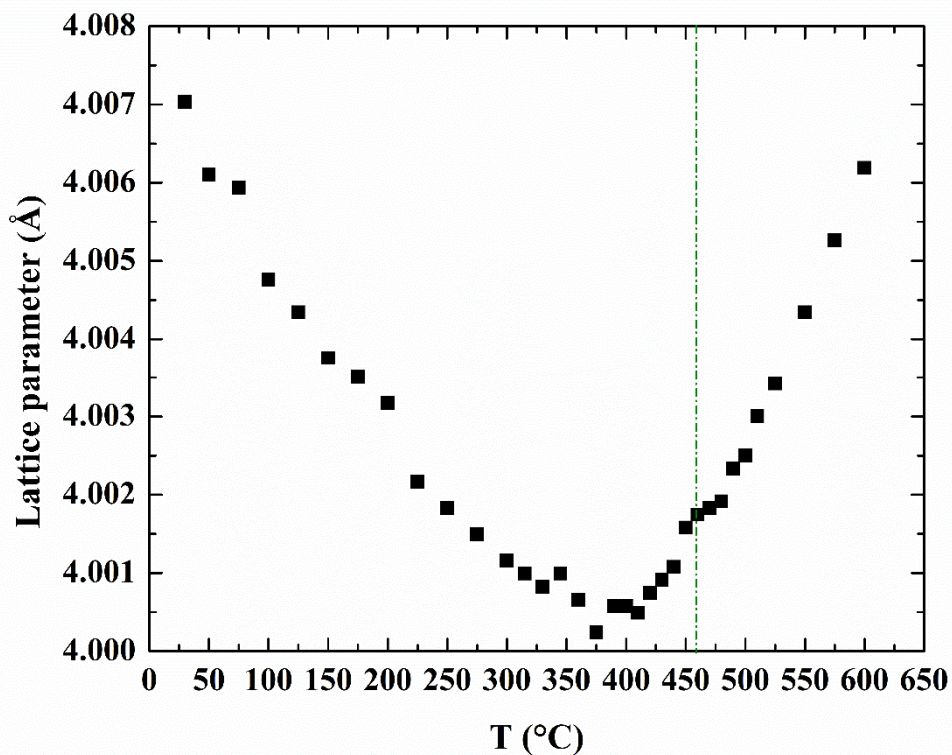
127 sample is our determination of the Curie temperature. In Fig 3 we plot the average c-axis

128 lattice parameter as a function of temperature. A decrease of this parameter, due to the

129 reduction of the out-of-plane component of polarization on approaching the
130 cubic/tetragonal phase transition, is observed. The Curie temperature is around 375 °C
131 and thus significantly lower than the reported value of 460°C for bulk PZT. This result is
132 not common in epitaxially grown thin films since strain is reported to push the transition
133 to higher temperature than in bulk. However bulk-like or even lower T_c values have been
134 reported in c- axis oriented thin films [2][14] and more recently in
135 ferroelectric/paraelectric PT-based SLs [15][16] despite epitaxial strain effects. Their
136 common feature is a destabilization of the ferroelectricity by the depolarizing field and
137 the resulting occurrence of 180° domains, at the origin of a lowering T_c which has also
138 been justified theoretically[17]. This feature is coherent with the detection of
139 nanodomains by XRD.

140

141



142

143 **Fig. 3.** Temperature dependence of the average out-of-plane c axis lattice parameter for
144 the ([PZT₅/STO₆]₁₀) SL. The dotted line marks the Curie temperature of bulk PZT.

145

146 **4. Conclusion**

147

148 The ferroelectric/paraelectric SLs constitute flexible model systems to investigate the
149 effects of strain and electrostatics on ferroelectric nanostructures like 180° domain
150 structure. XRD is commonly used to evidence 180° stripe domains through the detection
151 of satellite peaks characteristics of the ferroelectric stripe period. Our XRD and TEM
152 investigations performed on a PZT/STO SL, clearly show that in such samples
153 characterized by a noticeable misfit strain, the detection of diffuse scattering peaks can
154 originate either from ferroelectric 180° nanodomains or from modulation related to elastic
155 relaxation. It is shown that TEM investigations are required to disentangle elastic
156 relaxation and ferroelectric domain contributions to in plane scattering profiles.

157

158 **Acknowledgements**

159

160 This work was supported by the region of Hauts de France and the European Fund for
161 Economic and Regional Development FEDER. We thank Prof. M. G. Karkut for useful
162 discussions.

163

164 **References**

165 [1] J. Íñiguez, P. Zubko, I. Luk'yanchuk, A. Cano, Nat. Rev. Mater. (2019).

166 [2] S.K. Streiffer, J.A. Eastman, D.D. Fong, C. Thompson, A. Munkholm, M.V. Ramana
167 Murty, O. Auciello, G.R. Bai, G.B. Stephenson, Thin Films, Phys. Rev. Lett. 89
168 (2002) 067601.

- 169 [3] R. Takahashi, O. Dahl, E. Eberg, J.K. Grepstad, T. Tybell, *J. Appl. Phys.* 104 (2008)
170 064109.
- 171 [4] P. Zubko, N. Jecklin, N. Stucki, C. Lichtensteiger, G. Rispens, J.-M. Triscone,
172 *Ferroelectrics*. 433 (2012) 127–137.
- 173 [5] N. Lemée, I.C. Infante, C. Hubault, A. Boulle, N. Blanc, N. Boudet, V. Demange,
174 M.G. Karkut, *ACS Appl. Mater. Interfaces*. 7 (2015) 19906–19913.
- 175 [6] A.K. Yadav, C.T. Nelson, S.L. Hsu, Z. Hong, J.D. Clarkson, C.M. Schlepütz, A.R.
176 Damodaran, P. Shafer, E. Arenholz, L.R. Dedon, D. Chen, A. Vishwanath, A.M.
177 Minor, L.Q. Chen, J.F. Scott, L.W. Martin, R. Ramesh, *Nature*. 530 (2016) 198–
178 201.
- 179 [7] V.M. Kaganer, O. Brandt, A. Trampert, K.H. Ploog, *Phys. Rev. B*. 72 (2005).
- 180 [8] A.H.G. Vlooswijk, B. Noheda, G. Catalan, A. Janssens, B. Barcones, G. Rijnders,
181 D.H.A. Blank, S. Venkatesan, B. Kooi, J.T.M. de Hosson, *Appl. Phys. Lett.* 91
182 (2007) 112901.
- 183 [9] C. Hubault, C. Davoisne, A. Boulle, L. Dupont, V. Demange, A. Perrin, B. Gautier,
184 J. Holc, M. Kosec, M.G. Karkut, N. Lemée, *J. Appl. Phys.* 112 (2012) 114102.
- 185 [10] A. Boulle, I.C. Infante, N. Lemée, *J. Appl. Crystallogr.* 49 (2016) 845–855.
- 186 [11] P. Zubko, N. Jecklin, A. Torres-Pardo, P. Aguado-Puente, A. Gloter, C.
187 Lichtensteiger, J. Junquera, O. Stéphan, J.-M. Triscone, *Nano Lett.* (2012).
- 188 [12] L.E. Shilkrot, D.J. Srolovitz, J. Tersoff, , *Appl. Phys. Lett.* 77 (2000) 304.
- 189 [13] C. Hubault, C. Davoisne, L. Dupont, A. Perrin, A. Boulle, J. Holc, M. Kosec, M.G.
190 Karkut, N. Lemée, *Appl. Phys. Lett.* 99 (2011) 052905.
- 191 [14] D.D. Fong, G.B. Stephenson, S.K. Streiffer, J.A. Eastman, O. Auciello, P.H. Fuoss,
192 C. Thompson, *Science*. 304 (2004) 1650–1653.
- 193 [15] P. Zubko, N. Stucki, C. Lichtensteiger, J.-M. Triscone, *Phys. Rev. Lett.* 104 (2010)
194 187601.

- 195 [16] P. Zubko, N. Jecklin, N. Stucki, C. Lichtensteiger, G. Rispens, J.-M. Triscone,
196 Ferroelectrics. 433 (2012) 127–137.
- 197 [17] G.B. Stephenson, K.R. Elder, J. Appl. Phys. 100 (2006) 051601-051601-17.
198